

# Lawrence Berkeley National Laboratory

## LBL Publications

### Title

Raising the Asymmetric Catalytic Efficiency of Chiral Covalent Organic Frameworks by Tuning the Pore Environment

### Permalink

<https://escholarship.org/uc/item/21k1h2mb>

### Journal

ACS Applied Materials & Interfaces, 16(8)

### ISSN

1944-8244

### Authors

Zhang, Kai

Tang, Xihao

Yang, Xi

et al.

### Publication Date

2024-02-28

### DOI

10.1021/acsami.3c17048

### Copyright Information

This work is made available under the terms of a Creative Commons Attribution License, available at <https://creativecommons.org/licenses/by/4.0/>

Peer reviewed

# Raising the Asymmetric Catalytic Efficiency of Chiral Covalent Organic Frameworks by Tuning the Pore Environment

Kai Zhang,<sup>†</sup> Xihao Tang,<sup>†</sup> Xi Yang,<sup>†</sup> Jialin Wu,<sup>†</sup> Baoying Guo,<sup>†</sup> Rui Xiao,<sup>†</sup> Yao Xie,<sup>†</sup> Shengrun Zheng,<sup>†,§</sup> Huawei Jiang,<sup>†,§</sup> Jun Fan,<sup>†,§</sup> Weiguang Zhang,<sup>†,§</sup> Yi Liu<sup>\*,‡</sup> and Songliang Cai<sup>\*,†,§</sup>

<sup>†</sup>*GDMPA Key Laboratory for Process Control and Quality Evaluation of Chiral Pharmaceuticals, and Guangzhou Key Laboratory of Analytical Chemistry for Biomedicine, School of Chemistry, South China Normal University, Guangzhou 510006, P. R. China*

<sup>‡</sup>*The Molecular Foundry, Lawrence Berkeley National Laboratory, Berkeley, California 94720, United States*

<sup>§</sup>*SCNU Qingyuan Institute of Science and Technology Innovation Co., Ltd., Qingyuan 511517, P. R. China*

**ABSTRACT:** Chiral covalent organic frameworks (COFs) hold considerable promise in the realm of heterogeneous asymmetric catalysis. However, fine-tuning the pore environment to enhance both the activity and stereoselectivity of chiral COFs in such applications remains a formidable challenge. In this study, we have successfully designed and synthesized a series of clover-shaped, hydrazone-linked chiral COFs, each with a varying number of accessible chiral pyrrolidine catalytic sites. Remarkably, the catalytic efficiencies of these COFs in the asymmetric aldol reaction between cyclohexanone and 4-nitrobenzaldehyde correlate well with the number of accessible pyrrolidine sites within the frameworks. The COF featuring nearly one pyrrolidine moiety at each nodal point demonstrated excellent reaction yields and enantiomeric excess (ee) values, reaching up to 97% and 83%, respectively. The findings not only underscore the profound impact of a deliberately controlled chiral pore environment on the catalytic efficiencies of COFs, but also offer a new perspective for the design and synthesis of advanced chiral COFs for efficient asymmetric catalysis.

**KEYWORDS:** chiral covalent organic frameworks, asymmetric catalysis, enhanced catalytic performance, pore environment tuning, clover-like topology, hydrazone-linked COF

## INTRODUCTION

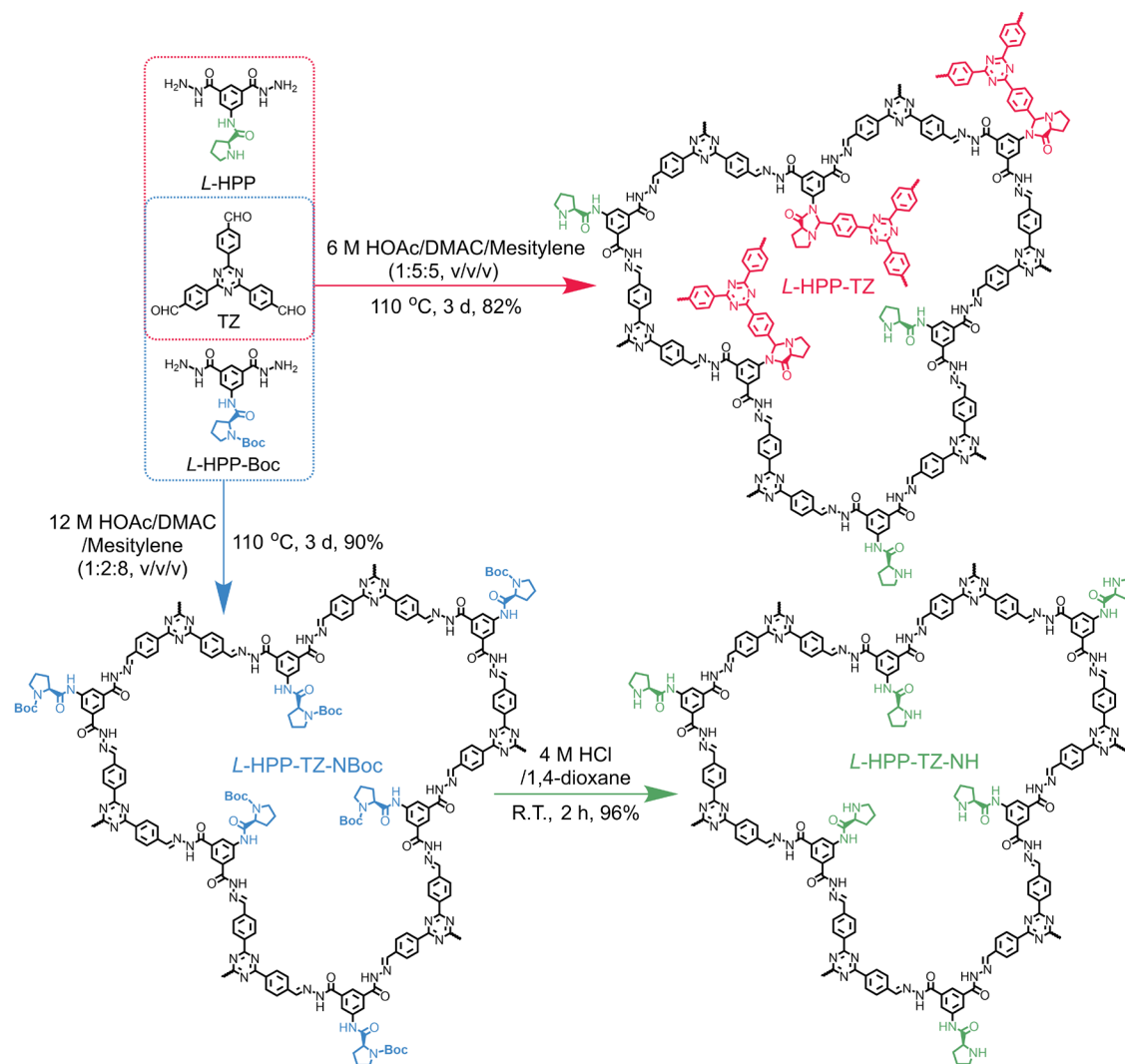
Chiral enantiomers often exhibit divergent physiological activities and distinct chemical selectivity, rendering the synthesis of compounds with specific chirality a critical undertaking. Asymmetric catalysis, as an ideal way to directly produce enantiomeric pure compounds, has garnered significant attention in recent years. Notably, proline and its derivatives — a representative class of chiral organocatalysts — exhibit excellent catalytic performance and chiral selectivity across a range of reactions, including Mannich reaction, Michael reaction, Morita-Baylis-Hillman reaction and aldol addition reaction.<sup>1,2</sup> To address challenges associated with catalyst recovery and product purification in chiral catalysis, these organocatalysts have been grafted onto solid supports to facilitate

heterogeneous catalytic transformations and subsequent catalyst regeneration. For example, enantiomerically pure proline moieties have been successfully incorporated into metal-organic frameworks (MOFs) through amide condensation.<sup>3,4</sup> However, the exposed pyrrolidine-NH active sites may engage in the coordination with metal ions during the self-assembly process, thereby compromising the catalyst's activity.<sup>1</sup> When protecting groups such as *tert*-butoxycarbonyl (Boc) were employed to mitigate such problems, the additional deprotection step, such as the post-synthetic thermal cleavage of Boc groups led to undesired racemization and severe attenuation of stereoselectivity.<sup>5</sup> Furthermore, the use of hazardous heavy metal ions in some MOFs poses additional environmental concerns. Therefore, the quest for metal-free, stable porous framework materials that can serve as reliable supports for organocatalytic moieties is of paramount importance.

Since the first report of covalent organic frameworks (COFs) in 2005,<sup>6</sup> such crystalline polymers have aroused significant interest due to their potential applications in various areas such as gas storage,<sup>7-9</sup> drug delivery,<sup>10-12</sup> chemical sensing,<sup>13-16</sup> pollutant adsorption,<sup>17-19</sup> electrochemistry,<sup>20-22</sup> chromatographic separation<sup>23-25</sup> and heterogeneous catalysis.<sup>26-28</sup> In particular, chiral COFs can be constructed by incorporating chiral structural moieties.<sup>29,30</sup> The outstanding properties of chiral COFs, including highly ordered porous structures, large specific surface area, excellent chemical stability and inherent chiral pore channels, position them as promising materials for enantiomeric separation,<sup>31-34</sup> chiral optics,<sup>35-38</sup> chiral recognition,<sup>39-41</sup> and heterogeneous asymmetric catalysis.<sup>42-46</sup> However, the rational design and construction of chiral COFs present considerable challenges and remain underexplored. These challenges primarily stem from the difficulty in reconciling asymmetry with the crystalline nature inherent to organic frameworks. Concerning their utility in asymmetric catalysis, the literature is limited mostly to imine-linked chiral COFs. For example, chiral pyrrolidine-functionalized imine-linked COFs were synthesized via covalent post-synthetic modification or *de novo* synthesis, and subsequently employed in chiral catalysis.<sup>44,47</sup> To the best of our knowledge, the application of chiral COFs featuring robust hydrazone linkages in asymmetric catalysis

remains unexplored. Furthermore, while significant strides have been made, a systematic study aimed at fine-tuning the pore environments of chiral COFs to optimize both catalytic activity and stereoselectivity is still an uncharted yet highly desirable research avenue.

**Scheme 1. Syntheses of chiral COFs *L*-HPP-TZ, *L*-HPP-TZ-NBoc, and *L*-HPP-TZ-NH.**



chiral linkers and explored their use as heterogeneous catalysts for the asymmetric aldol reaction between cyclohexanone and nitrobenzaldehydes. We have demonstrated that the density of NH active sites of pyrrolidine in the pore channels of chiral COFs can be regulated by the introduction of Boc protecting groups, which dictates the asymmetric catalytic efficiency of the model aldol reaction, giving rise to excellent reaction yield and ee value.

## RESULTS AND DISCUSSION

**Synthesis and Characterization.** In our ligand design, the chiral ligand *L*-HPP was obtained in high yield from the stepwise reaction of dimethyl 5-aminoisophthalate with hydrazine and *L*-proline (Scheme S1b). The two acylhydrazine units were arranged with a bent angle of around 120° off the central 1,3-disubstituted benzene core, from which a clover-type of COF was expected when condensed with a  $C_3$  symmetric trialdehyde monomer TZ (Scheme 1). It is worth noting that this 1,3-substitution pattern was adopted over the 1,4-substitution

Herein, we designed and prepared a series of clover-like hydrazone-linked chiral COFs using nonlinear pyrrolidine-containing

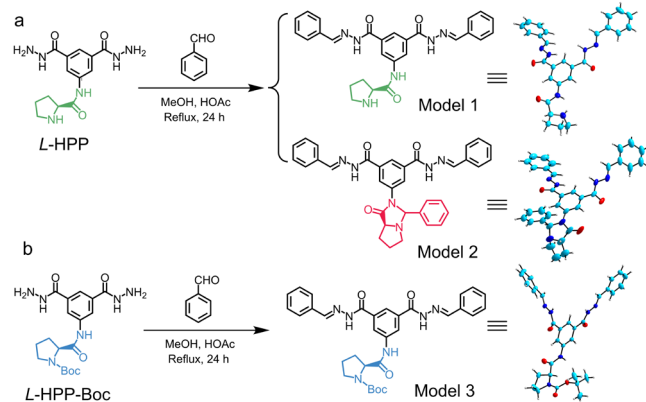
pattern where the two acylhydrazine units are linearly aligned, to avoid the complications of spontaneous ring closure reaction between one of the acylhydrazine units and the adjacent amino group, as described previously (Scheme S1a).<sup>37</sup>

When *L*-HPP was subjected to the reaction with the trialdehyde monomer TZ in a molar ratio of 2:3 under solvothermal conditions (in degassed aqueous acetic acid (6 M)/dimethylacetamide/mesitylene (1:5:5, v/v/v), 110 °C, 3 days, see Supporting Information), a semicrystalline COF powder was obtained (Scheme 1), which, when employed in the asymmetric aldol condensation reaction, exhibited very low chiral catalytic activity (see details later). In order to verify if the proline catalytic sites were intact and remained accessible in the resultant COF, *L*-HPP was subjected to the reaction with the monovalent benzaldehyde. During the experiment, an equal amount of acetic acid was added as a catalyst, similar to the conditions employed for COF synthesis. Despite a starting molar ratio of 1:2 for *L*-HPP and benzaldehyde, two different condensation products, Model 1 and Model 2, were obtained (Scheme 2a) in a ratio close to 1:1, as revealed by <sup>1</sup>H NMR spectroscopy (Figure S1).

Single-crystal X-ray diffraction analysis clearly revealed that Model 2 was an adduct of Model 1 with an additional benzaldehyde (Scheme 2a and Table S1), in which the active pyrrolidine-NH group underwent a cyclization reaction with benzaldehyde and the N atom of the amide unit. The tendency for ring-annulation in Model 2 may account for the unexpected reactivity of pyrrolidine towards aromatic aldehydes. Correspondingly, the pyrrolidine units in *L*-HPP may have engaged in the reaction with the aldehyde groups in TZ during the COF synthesis, resulting in the formation of *L*-HPP-TZ with partially blocked pyrrolidine sites (Scheme 1).

The *N*-Boc protected *L*-HPP-Boc linker was then synthesized and employed in the model reaction with benzaldehyde and the COF synthesis with TZ (Scheme 1). From the model reaction carried out under the same acidic reaction conditions, the Boc-containing Model 3 was obtained as the sole product (Scheme 2b) with no sign of the ring-closure Model 2 product, verifying that the Boc group was robust and remained intact under the acidic conditions. From the solvothermal condensation reaction between *L*-HPP-Boc and TZ, *L*-HPP-TZ-NBoc COF was successfully obtained as a pale-yellow solid. Further deprotection by treating *L*-HPP-TZ-NBoc with 4 M HCl/1,4-dioxane was successfully implemented, giving rise to *L*-HPP-TZ-NH COF containing exposed pyrrolidine-NH catalytic sites (Scheme 1). When *L*-HPP-TZ-NH was used to catalyze the same asymmetric aldol reaction, the catalytic ability and chiral selectivity were significantly improved (described below).

**Scheme 2.** Syntheses of the model compounds (a) Model 1 and Model 2, and (b) Model 3, the structures of which were verified by their corresponding single-crystal structures shown on the right.



The crystallinity and framework structures of the obtained chiral COFs were characterized by powder X-ray diffraction (PXRD) analysis. As illustrated in Figure 1a, all the PXRD patterns of *L*-HPP-TZ, *L*-HPP-TZ-NBoc, and *L*-HPP-TZ-NH exhibited a relatively intense diffraction peak at about 5.0°, which could be assigned to the reflection from the (110) facet. Additionally, the other two weak peaks at around 7.9° and 26.2° can be attributed to the (300) and (003) facets, respectively. Structural simulations of *L*-HPP-TZ-NH considered three common packing models including AA packing (Figure 1b, Table S6), AB packing (Figure 1c, Table S7) and ABC packing (Figure 1d, Table S8). The results indicated that the experimental PXRD pattern of *L*-HPP-TZ-NH matched much better with the calculated PXRD pattern generated from the ABC stacking mode than those of the AA stacking and AB stacking modes (Figure 1a). Such an ABC packing structure of *L*-HPP-TZ-NH was similar to those of the other reported achiral clover-like imine-linked COFs.<sup>48,49</sup> Thus, the suggested model with ABC packing structure was subsequently subjected to the Pawley refinement, producing a PXRD pattern that was in good agreement with the experiment (Figure S2). The Pawley refinement gave rise to cell parameters of  $a = b = 35.20 \text{ \AA}$ ,  $c = 10.63 \text{ \AA}$ ,  $\alpha = \beta = 90^\circ$ ,  $\gamma = 120^\circ$ , and reasonable final factors  $R_{wp} = 2.76\%$  and  $R_p = 2.20\%$ . The PXRD patterns of *L*-HPP-TZ and *L*-HPP-TZ-NBoc were similar to that of *L*-HPP-TZ-NH in terms of peak positions and intensities, indicating that all of these COFs possessed similar framework structures with ABC packing modes (Figures 1d-1f). It is worth noting that despite that different synthesis conditions were attempted to enhance the crystallinity of these COFs, their PXRD patterns could not be improved further, presumably due to the existence of the bulky pendant proline-based chiral groups in the COF structures, which might greatly affect the  $\pi$ - $\pi$  stacking interactions and thus resulting in the staggered alignment between the neighboring layers.<sup>29</sup> So far, only few achiral COFs with the interesting clover-like topology have been reported.<sup>48-50</sup> To the best of our knowledge, the hydrazone-linked COFs in this work represent the first examples of clover-like chiral COFs.

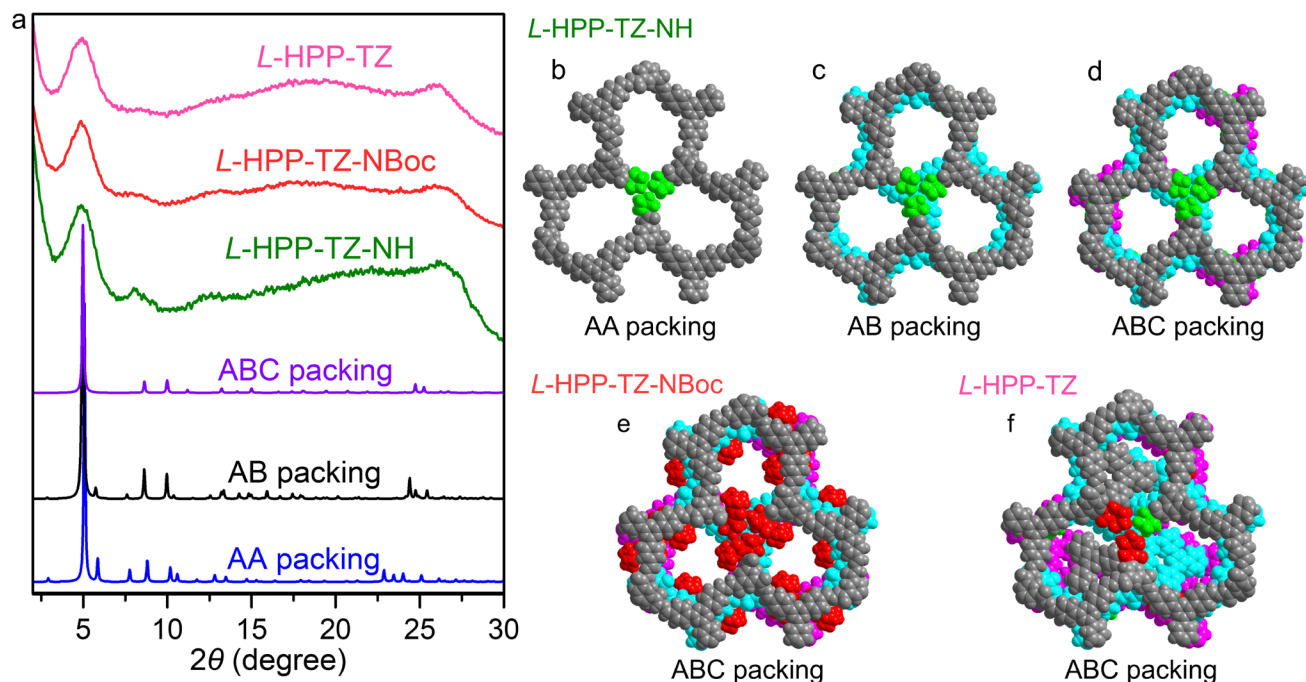


**Figure 1.** (a) Simulated PXRD patterns of *L*-HPP-TZ-NH: AA packing (blue), AB packing (black) and ABC packing (purple) structures; Experimental PXRD patterns of *L*-HPP-TZ-NH (green), *L*-HPP-TZ-NBoc (red) and *L*-HPP-TZ (pink). (b) Simulated structure of *L*-HPP-TZ-NH with AA packing. (c) Simulated structure of *L*-HPP-TZ-NH with AB packing. (d) Simulated structure of *L*-HPP-TZ-NH with ABC packing. (e) Simulated structure of *L*-HPP-TZ-NBoc with ABC packing. (f) Illustration of partial structure of *L*-HPP-TZ with ABC packing. The active pyrrolidine-NH units were highlighted in green, while the blocked pyrrolidine-NH sites were highlighted in red.

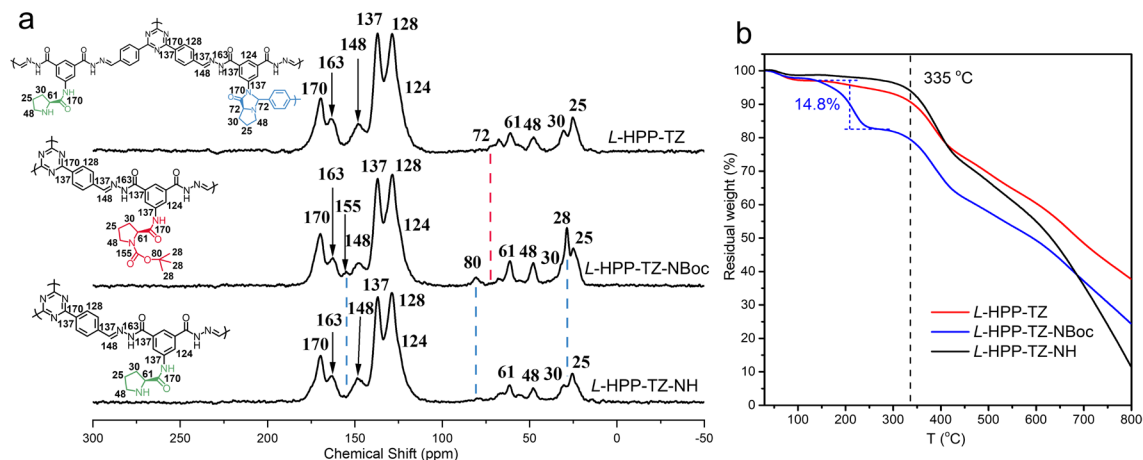


**Figure 2.** (a) Solid-state <sup>13</sup>C CP-MAS NMR spectra of *L*-HPP-TZ, *L*-HPP-TZ-NBoc, and *L*-HPP-TZ-NH. (b) TGA curves of *L*-HPP-TZ (red), *L*-HPP-TZ-NBoc (blue) and *L*-HPP-TZ-NH (black). The significant weight loss (14.8%) in the region of 145–273 °C in the TGA curve of *L*-HPP-TZ-NBoc (blue) corresponds to the cleavage of Boc groups (theoretical mass loss: 15.8%).

All three chiral COFs were characterized by Fourier transform infrared spectroscopy (FT-IR), which were similar due to their related framework structures (Figure S5). The spectra of these COFs revealed the nearly complete absence of the characteristic aldehyde stretching (1700 cm<sup>-1</sup>) of TZ and the weak amino stretching (3400–3200 cm<sup>-1</sup>) of the starting chiral building blocks. The characteristic C=N (1600 cm<sup>-1</sup>) stretching bands, which was also featured in the FT-IR spectra of the corresponding model compounds, were observed for the obtained COFs, signifying the completion of the Schiff-base reaction (Figures S3 and S4). Further chemical information was revealed by <sup>13</sup>C cross-polarization magic-angle spinning (CP-MAS) NMR analysis (Figure 2a). The <sup>13</sup>C CP-MAS NMR spectra showed the

characteristic peak for the imine carbon at 148 ppm for all the chiral COFs, confirming the formation of C=N bonds. The chemical shifts of other fragments were in good agreement with those of the monomers. Notably, the emerging resonance at 72 ppm for *L*-HPP-TZ could be due to the formation of annulated rings from the ring-closure reaction between pyrrolidine-NH and TZ. The peaks at 61, 48, 30, and 25 ppm were assigned to the carbon atoms attached to the chiral pyrrolidine group. Additionally, the disappearance of the signals at 155, 80, and 28 ppm for *L*-HPP-TZ-NH, was indicative of the successful removal of the Boc protecting groups.

Thermogravimetric analysis (TGA) revealed that these chiral COFs presented good thermal stabilities up to ~335 °C (Figure

2b). In the case of *L*-HPP-TZ-NBoc, an additional weight loss of ~14.8% was observed in the region of 145–273 °C, accounting for the cleavage of Boc groups (theoretical value: 15.8%). In addition, no apparent weight loss was observed for *L*-HPP-TZ-NH at ~270 °C, further proving that the Boc groups were successfully removed.<sup>4,44</sup> Scanning electron microscopy (SEM) images revealed that *L*-HPP-TZ exhibited a rod-shaped morphology with some nanoparticles on the surface (Figure 3a), while both *L*-HPP-TZ-NBoc and *L*-HPP-TZ-NH displayed rod-shaped morphologies with much smoother surfaces (Figures 3b–3c). The specific surface area and pore size distribution of the three COFs were studied by N<sub>2</sub> adsorption–desorption experiments at 77 K. The adsorption curves of all three chiral COFs exhibited the type-IV sorption isotherms, indicating their porous nature (Figure 3d). The adsorption curve of *L*-HPP-TZ showed a rapid increase at low relative pressure ( $P/P_0 < 0.1$ ), suggesting the presence of micropores. A rise in the isotherm at higher relative pressures (0.8–0.99  $P/P_0$ ) occurred, ascribed to the presence of textural mesopores caused by agglomeration of the COF crystals.<sup>51</sup> The Brunauer–Emmett–Teller (BET) surface areas of *L*-HPP-TZ, *L*-HPP-TZ-NBoc and *L*-HPP-TZ-NH were found to be 41.6, 16.3, and 35.2 m<sup>2</sup>/g, respectively (Figures S6–S8). Such limited BET surface areas might be attributable to the ABC packing mode and relatively low crystallinity of the resulting chiral COFs. The nonlocal density functional theory (NLDFT) simulation indicated narrow aperture distributions, with the average pore width of 1.42, 2.02 and 2.02 nm for *L*-HPP-TZ, *L*-HPP-TZ-NBoc and *L*-HPP-TZ-NH, respectively (Figures S9–S11). The decrease of average pore width for *L*-HPP-TZ was due to blocked pore channels caused by the ring-closure reaction between pyrrolidine group of *L*-HPP and aldehyde monomer. To further study the chemical stability of the hydrazone-linked COFs, *L*-HPP-TZ-NH was selected as an example and immersed in common solvents for 7 days. As indicated by PXRD, *L*-HPP-TZ-NH treated with different solvents including dimethyl sulfoxide (DMSO), dichloromethane (DCM), tetrahydrofuran (THF), methanol (MeOH), *N,N*-dimethylformamide (DMF), H<sub>2</sub>O, 4 M NaOH (aq) and 4 M HCl (aq), still retained its crystallinity after a one-week treatment (Figure S12). The high chemical stability of *L*-HPP-TZ-NH was mainly attributed to the formation of robust hydrazone linkage in the framework. Additionally, the circular dichroism (CD) spectra of *L/D*-HPP-TZ, *L/D*-HPP-TZ-NBoc and *L/D*-HPP-TZ-NH chiral COFs synthesized by *L/D*-HPP and *L/D*-HPP-Boc enantiomeric building blocks showed mirror symmetric correlation, which indicated their enantiomeric properties (Figures S13–S15).

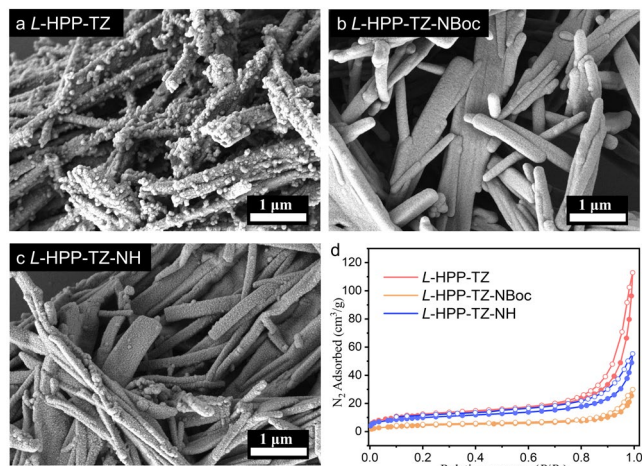


**Figure 3.** (a) The SEM image of *L*-HPP-TZ. (b) The SEM image of *L*-HPP-TZ-NBoc. (c) The SEM image of *L*-HPP-TZ-NH. (d) The N<sub>2</sub>

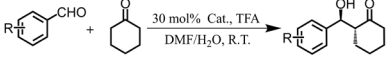
sorption isotherms of *L*-HPP-TZ (red), *L*-HPP-TZ-NBoc (yellow), and *L*-HPP-TZ-NH (blue).

**Asymmetric Catalysis.** The obtained chiral COFs exhibited similar framework structures but different chiral pore channel functionalities, which allowed us to investigate the impact of the pore environments on the activities and stereoselectivities of the resultant chiral COFs in asymmetric catalysis. The chiral COFs were used as catalysts for asymmetric aldol reaction, which is one of the most classical carbon-carbon bond forming reactions in organic synthesis.<sup>52,53</sup> Since the solvent is a crucial factor, we initially investigated the catalytic activity of *L*-HPP-TZ-NH for the aldol reaction of cyclohexanone with 4-nitrobenzaldehyde in various solvents. As displayed in Table S2, the aldol reactions catalyzed by *L*-HPP-TZ-NH for 4 days afforded the products in extremely low yields when THF, EtOH or toluene were utilized (entries 1–3 in Table S2). The use of DMF or H<sub>2</sub>O alone could only slightly increase the yields (entries 4 and 5 in Table S2), while moderately high yield was achieved when using DMF/H<sub>2</sub>O as the cosolvent (entry 6 in Table S2). Next, the impacts of acidic and basic additives on the asymmetric aldol reactions were studied. When acetic acid was used as the auxiliary acid agent, the catalytic activity of *L*-HPP-TZ-NH for the reaction of cyclohexanone with 4-nitrobenzaldehyde was the highest at room temperature, and a 98% yield was obtained after 4 days of reaction, while the corresponding ee value and dr value were 51% and 1:6.1, respectively (entry 7 in Table S2). When benzoic acid and *p*-toluenesulfonic acid were employed as auxiliary acid agents, the aldol reaction afforded the products in 97% and 61% yields, 61% and 74% ee values, and 1:4.8 and 1:13.5 dr values, respectively (entries 8 and 9 in Table S2). When trifluoroacetic acid was used as an agent, the products exhibited the highest ee and dr values up to 85% and 1:19.1, respectively (entry 6 in Table S2), despite a relatively low yield of 49%. In case of the basic additives, the use of Et<sub>3</sub>N and NaHCO<sub>3</sub> could significantly improve the yield of the products, while negligible ee values were detected (entries 10 and 11 in Table S2). When pyridine was employed as a basic additive, moderate yield and ee value of the aldol product were observed (entry 12 in Table S2). Meanwhile, the effects of catalyst loading, temperature and reaction time on the asymmetric aldol reactions were also explored. With the increase of the catalyst loading from 10 to 20 mol%, the yield of the aldol product increased notably from 26 to 42% (entries 1 and 2 in Table S3), while further increasing the catalyst loading up to 30 mol% only led to the slight increase of the yield (entry 6 in Table S3). When raising the temperature from room temperature to 45 and 60 °C, the reaction could be speeded up, but much lower ee values were observed (entries 3–5 in Table S3). Besides, the yield of the aldol product could be greatly improved with the increase of the reaction time (entries 5–7 in Table S3).

Particularly, extending the reaction time to 7 days resulted in an increased yield of 97%, while the ee value was well maintained (83%) and a dr value of 1:8.5 was achieved (entry 1 in Table 1, Figures S17 and S18). Under the same optimized reaction conditions, the catalytic activity and chiral selectivity of *L*-HPP-TZ-NBoc were inferior, with a poor 21% yield and a 9% ee value (entry 2 in Table 1, Figures S19 and S20), whereas the use of *L*-HPP-TZ as the catalyst only afforded a slightly higher yield of 39% and a 20% ee value (entry 3 in Table 1, Figures S21 and S22). The above catalytic experimental results indicated that the catalytic performances of the three chiral COFs were in the order of *L*-HPP-TZ-NH > *L*-HPP-TZ > *L*-HPP-TZ-NBoc (Figure 4). Compared with the catalytic activity and chiral selectivity of *L*-HPP-TZ-NBoc and *L*-HPP-TZ COFs, the catalytic activity of *L*-HPP-TZ-NH COF was increased by 4.6 and 2.5 times, and the chiral selectivity was increased by 9.2 and 4.2 times,

respectively. The worst catalytic ability of *L*-HPP-TZ-NBoc was in accordance with its least accessible catalytic sites in the framework due to Boc protection. The catalytic efficiency of *L*-HPP-TZ COF was also low, due to the limited amount of exposed pyrrolidine-NH active sites after ring annulation between amidopyrrolidine and aldehyde groups. In contrast, the

**Table 1.** Asymmetric Aldol Reactions Catalyzed by the Clover-Like Hydrazone-Linked Chiral COFs and Model 1.



entry <sup>a</sup>	catalyst	R	yield/% <sup>b</sup>	ee/% <sup>c</sup>	syn/anti <sup>d</sup>
1	<i>L</i> -HPP-TZ-NH	4-NO <sub>2</sub>	97	83	1:8.5
2	<i>L</i> -HPP-TZ-NBoc	4-NO <sub>2</sub>	21	9	1:1.0
3	<i>L</i> -HPP-TZ	4-NO <sub>2</sub>	39	20	1:4.3
4	Model 1 <sup>e</sup>	4-NO <sub>2</sub>	86	19	1.9.5
5	<i>L</i> -HPP-TZ-a1	4-NO <sub>2</sub>	36	15	1:1.9
6	<i>L</i> -HPP-TZ-a2	4-NO <sub>2</sub>	33	9	1:1.6
7	<i>L</i> -HPP-TZ-NH	3-NO <sub>2</sub>	82	80	1:6.7
8	<i>L</i> -HPP-TZ-NBoc	3-NO <sub>2</sub>	17	13	1:1.4
9	<i>L</i> -HPP-TZ	3-NO <sub>2</sub>	29	19	1:2.0
10	<i>L</i> -HPP-TZ-NH	2-NO <sub>2</sub>	40	74	1:16.7

<sup>a</sup>Reaction conditions: aldehyde (0.10 mmol), ketone (0.3 mL), chiral COFs (0.03 mmol), TFA (0.03 mmol), and DMF/H<sub>2</sub>O (1 mL/0.3 mL) at R.T. for 7 days. <sup>b</sup>Isolated yield. <sup>c</sup>Determined by chiral HPLC. <sup>d</sup>Determined by <sup>1</sup>H NMR spectroscopy. <sup>e</sup>Catalyzed by 0.03 mmol Model 1 as the homogeneous counterpart.

catalytic efficiency of *L*-HPP-TZ-NH was the best since almost all pyrrolidine-NH catalytic sites were well retained in the framework structure. To further study the influence of the reduction of active sites on the catalytic performance, we increased the molar ratio of TZ and *L*-HPP to 3:3 and 4:3, which only resulted in the formation of corresponding amorphous *L*-HPP-TZ-a1 and *L*-HPP-TZ-a2 (Figures S25 and S26). The lack of crystallinity for *L*-HPP-TZ-a1 and *L*-HPP-TZ-a2 might be attributed to extensive reaction of the pyrrolidine-NH sites with the excess TZ aldehyde monomer, which hindered crystallization. When *L*-HPP-TZ-a1 and *L*-HPP-TZ-a2 were used to catalyze the reaction of 4-nitrobenzaldehyde with cyclohexanone, the corresponding yields were further decreased to 36% and 33%, and the ee values were reduced to 15% and 9%, respectively (entries 5 and 6 in Table 1). For comparison, we used Model 1 as the homogeneous counterpart of COF catalysts and examined its catalytic activity under the same conditions. The results uncovered that Model 1 afforded a yield of 86% and an ee value of 19% (entry 4 in Table 1, Figures S23 and S24). The superior catalytic activity and enantioselectivity of *L*-HPP-TZ-NH than Model 1 could be due to multiple chiral inductions in the confined space of the COF heterogeneous catalyst. Indeed, the reported COFs for asymmetric catalysis mainly focus on imine-based chiral COFs, while the application of chiral COFs containing robust hydrazone linkages in asymmetric catalysis has never been documented. This work, to the best of our knowledge, represents the first example of the construction of hydrazone-linked chiral COFs for asymmetric catalysis. The asymmetric catalytic ability of the pyrrolidine-containing chiral *L*-HPP-TZ-NH COF was compared with the other reported chiral pyrrolidine functionalized COFs and MOFs. As illustrated in Table S4, the asymmetric catalytic performance of *L*-HPP-TZ-NH COF for the aldol condensation reaction of cyclohexanone and 4-nitrobenzaldehyde was comparable or even higher than those of the reported DMTA-TPB1/*n*' COFs (*n* = 2, 3, and 4) containing pyrrolidine units.<sup>43</sup> Moreover, the asymmetric catalytic ability of *L*-HPP-TZ-NH COF, especially the catalytic stereoselectivity, surpassed most of the documented proline-MOFs such as *S*-Cd-MOF,<sup>54</sup> RR-DUT-136-amine,<sup>55</sup> UiO-66-LP-120,<sup>56</sup> UiO-68-NHPro,<sup>57</sup> Ap@3,<sup>58</sup>

Cd-TBT,<sup>59</sup> and CMIL-1-Pro,<sup>60</sup> rendering it a promising catalyst for efficient asymmetric catalysis of aldol reactions.

To investigate the generality of these chiral COFs catalysts, the scope of substrates was subsequently investigated. When the substrate was replaced with 3-nitrobenzaldehyde, the yield, ee value and dr value of the reactions catalyzed by *L*-HPP-TZ were 82%, 80% and 1:6.7, respectively (entry 7 in Table 1, Figures S28 and S29). However, *L*-HPP-TZ-NBoc and *L*-HPP-TZ displayed only 17% and 29% yields, 13% and 19% ee values, and 1:1.4 and 1:2 dr values (entries 8 and 9 in Table 1). While the substrate was replaced with 2-nitrobenzaldehyde, the *L*-HPP-TZ-NH catalyst could still afford the product with ee value and dr value up to 74% and 1:16.7 (entry 10 in Table 1, Figures S31 and S32), although the yield was only 40% due to the steric hindrance of ortho nitro group. Recycling tests also proved the heterogeneous nature of *L*-HPP-TZ-NH and its ability to be re-used in asymmetric aldol reaction ( $\geq 90\%$  yield and 83%, 77% and 70% ee for 1–3 cycles, respectively) (Table S5, Figures S33–S35). After three repeated uses, PXRD measurements showed that *L*-HPP-TZ-NH COF still maintained good crystallinity, indicating the high chemical stability of the chiral COF owing to the robust hydrazone linkages in the framework (Figure S36).

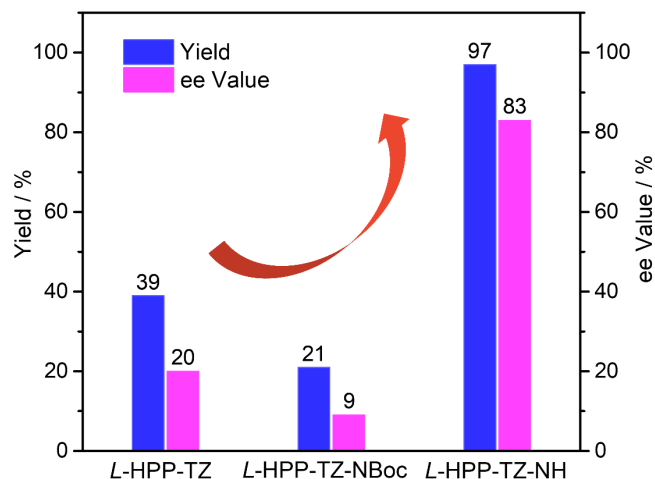


**Figure 4.** Improved asymmetric catalytic performance of *L*-HPP-TZ, *L*-HPP-TZ-NBoc and *L*-HPP-TZ-NH chiral COFs for asymmetric aldol reaction by tuning the pore environment.

## CONCLUSIONS

In conclusion, we have designed and synthesized three clover-like hydrazone-linked chiral COFs containing various copies of exposed chiral pyrrolidine units. When used in catalytic asymmetric aldol reactions, the catalytic activity and chiral selectivity of these chiral COFs were closely related to their pore environments. *L*-HPP-TZ-NH containing the largest number of pyrrolidine-NH active sites in the pore channels exhibited the highest catalytic activity (97% yield) and chiral selectivity (83% ee and 1:8.5 dr) for catalyzing the reactions between cyclohexanone and nitrobenzaldehydes. *L*-HPP-TZ-NBoc and *L*-HPP-TZ with completely and partially blocked pyrrolidine-NH sites in the pores, respectively, showed poor chiral catalytic performances. The results not only indicate that deliberately controlled chiral pore environment in COFs can significantly attenuate their asymmetric catalytic efficiencies, but also provide a new perspective for the design and construction of novel chiral COFs for efficient asymmetric catalysis.

## ASSOCIATED CONTENT

**Supporting Information.** The Supporting Information is available free of charge on the ACS Publications website at <https://pubs.acs.org/doi/xxxxxxx>. Full synthetic procedure, FT-IR, N<sub>2</sub> sorption isotherms, PXRD, CD spectra, LC-MS, <sup>1</sup>H NMR and <sup>13</sup>C NMR, as well as tables for the fractional atomic coordinates of the simulated COFs (PDF).

**Accession Codes.** CCDC deposition numbers 2285485-2285487 contain the supplementary crystallographic data for this paper. These data can be acquired free-of-charge via [www.ccdc.cam.ac.uk/data\\_request/cif](http://www.ccdc.cam.ac.uk/data_request/cif), or by emailing [data-request@ccdc.cam.ac.uk](mailto:data-request@ccdc.cam.ac.uk), or by contacting the Cambridge Crystallographic Data Centre, 12 Union Road, Cambridge CB2 1EZ, UK; fax: +44 1223 336033.

## AUTHOR INFORMATION

### Corresponding Authors

\*E-mail: [songliangcai@m.scnu.edu.cn](mailto:songliangcai@m.scnu.edu.cn) (S. C.).

\*E-mail: [yliu@lbl.gov](mailto:yliu@lbl.gov) (Y.L.).

### Notes

The authors declare no competing financial interest.

## ACKNOWLEDGMENT

We gratefully acknowledge the financial support from the National Natural Science Foundation of P. R. China (Grant Nos. 22171092, 22073032 and 92056113), the Natural Science Foundation of Guangdong Province (Grant Nos. 2021A1515010211 and 2022A1515011243), and the Shenzhen Science and Technology Program (Grant No. CJGJZD20210408091800002). Y.L. acknowledges the support from the Molecular Foundry, a user facility supported by the Office of Science, Office of Basic Energy Sciences, of the U.S. Department of Energy under Contract No. DE-AC02-05CH11231.

## REFERENCES

- Zhou, M.; El-Sayed, E.-S. M.; Ju, Z.; Wang, W.; Yuan, D. The Synthesis and Applications of Chiral Pyrrolidine Functionalized Metal–Organic Frameworks and Covalent–Organic Frameworks. *Inorg. Chem. Front.* **2020**, *7*, 1319–1333.
- List, B. Enamine Catalysis Is a Powerful Strategy for the Catalytic Generation and Use of Carbanion Equivalents. *Acc. Chem. Res.* **2004**, *37*, 548–557.
- Kutzscher, C.; Hoffmann, H. C.; Krause, S.; Stoeck, U.; Senkowska, I.; Brunner, E.; Kaskel, S. Proline Functionalization of the Mesoporous Metal–Organic Framework DUT-32. *Inorg. Chem.* **2015**, *54*, 1003–1009.
- Lun, D. J.; Waterhouse, G. I.; Telfer, S. G. A General Thermolabile Protecting Group Strategy for Organocatalytic Metal–Organic Frameworks. *J. Am. Chem. Soc.* **2011**, *133*, 5806–5809.
- Ingleston, M. J.; Bacsá, J.; Rosseinsky, M. J. Homochiral H-Bonded Proline Based Metal Organic Frameworks. *Chem. Commun.* **2007**, *29*, 3036–308.
- Cote, A. P.; Benin, A. I.; Ockwig, N. W.; O’Keeffe, M.; Matzger, A. J.; Yaghi, O. M. Porous, Crystalline, Covalent Organic Frameworks. *Science* **2005**, *310*, 1166–1170.
- Singh, G.; Lee, J.; Karakoti, A.; Bahadur, R.; Yi, J.; Zhao, D.; Al-Bahily, K.; Vinu, A. Emerging Trends in Porous Materials for CO<sub>2</sub> Capture and Conversion. *Chem. Soc. Rev.* **2020**, *49*, 4360–4404.
- Mercado, R.; Fu, R.-S.; Yakutovich, A. V.; Talirz, L.; Haranczyk, M.; Smit, B. In Silico Design of 2D and 3D Covalent Organic Frameworks for Methane Storage Applications. *Chem. Mater.* **2018**, *30*, 5069–5086.
- Li, Z.; Zhi, Y.; Feng, X.; Ding, X.; Zou, Y.; Liu, X.; Mu, Y. An Azine-Linked Covalent Organic Framework: Synthesis, Characterization and Efficient Gas Storage. *Chem. Eur. J.* **2015**, *21*, 12079–12084.
- Fang, Q.; Wang, J.; Gu, S.; Kaspar, R. B.; Zhuang, Z.; Zheng, J.; Guo, H.; Qiu, S.; Yan, Y. 3D Porous Crystalline Polyimide Covalent Organic Frameworks for Drug Delivery. *J. Am. Chem. Soc.* **2015**, *137*, 8352–8355.
- Mitra, S.; Sasmal, H. S.; Kundu, T.; Kandambeth, S.; Illath, K.; Diaz Diaz, D.; Banerjee, R. Targeted Drug Delivery in Covalent Organic Nanosheets (CONs) via Sequential Postsynthetic Modification. *J. Am. Chem. Soc.* **2017**, *139*, 4513–4520.
- Wu, M. X.; Yang, Y. W. Applications of Covalent Organic Frameworks (COFs): From Gas Storage and Separation to Drug Delivery. *Chinese Chem. Lett.* **2017**, *28*, 1135–1143.
- Chen, G.; Lan, H. H.; Cai, S. L.; Sun, B.; Li, X. L.; He, Z. H.; Zheng, S. R.; Fan, J.; Liu, Y.; Zhang, W. G. Stable Hydrazone-Linked Covalent Organic Frameworks Containing O,N,O'-Chelating Sites for Fe(III) Detection in Water. *ACS Appl. Mater. Interfaces* **2019**, *11*, 12830–12837.
- Liu, X.; Huang, D.; Lai, C.; Zeng, G.; Qin, L.; Wang, H.; Yi, H.; Li, B.; Liu, S.; Zhang, M.; Deng, R.; Fu, Y.; Li, L.; Xue, W.; Chen, S. Recent Advances in Covalent Organic Frameworks (COFs) as a Smart Sensing Material. *Chem. Soc. Rev.* **2019**, *48*, 5266–5302.
- Meng, Z.; Mirica, K. A. Covalent Organic Frameworks as Multifunctional Materials for Chemical Detection. *Chem. Soc. Rev.* **2021**, *50*, 13498–13558.
- She, P.; Qin, Y.; Wang, X.; Zhang, Q., Recent Progress in External-Stimulus-Responsive 2D Covalent Organic Frameworks. *Adv. Mater.* **2022**, *34*, 2101175.
- Kang, F.; Wang, X.; Chen, C.; Lee, C. S.; Han, Y.; Zhang, Q. Construction of Crystalline Nitrene-Linked Covalent Organic Frameworks Via Kröhnke Oxidation. *J. Am. Chem. Soc.* **2023**, *145*, 15465–15472.
- Zhang, S. Y.; Tang, X. H.; Yan, Y. L.; Li, S. Q.; Zheng, S.; Fan, J.; Li, X.; Zhang, W. G.; Cai, S. Facile and Site-Selective Synthesis of an Amine-Functionalized Covalent Organic Framework. *ACS Macro Lett.* **2021**, *10*, 1590–1596.
- Li, R.; Tang, X.; Wu, J.; Zhang, K.; Zhang, Q.; Wang, J.; Zheng, J.; Zheng, S.; Fan, J.; Zhang, W.; Li, X.; Cai, S. A Sulfonate-Functionalized Covalent Organic Framework for Record-High Adsorption and Effective Separation of Organic Dyes. *Chem. Eng. J.* **2023**, *464*, 142706.
- Sun, J.; Xu, Y.; Lv, Y.; Zhang, Q.; Zhou, X. Recent Advances in Covalent Organic Framework Electrode Materials for Alkali Metal-Ion Batteries. *CCS Chemistry* **2023**, *5*, 1259–1276.
- Li, X.; Wang, H.; Chen, H.; Zheng, Q.; Zhang, Q.; Mao, H.; Liu, Y.; Cai, S.; Sun, B.; Dun, C.; Gordon, M.; Zheng, H.; Reimer, J.; Urban, J.; Ciston, J.; Tan, T.; Chan, E.; Zhang, J.; Liu, Y. Dynamic Covalent Synthesis of Crystalline Porous Graphitic Frameworks. *Chem.* **2020**, *6*, 933–944.
- Zhao, X. J.; Pachfule, P.; Thomas, A. Covalent Organic Frameworks (COFs) for Electrochemical Applications. *Chem. Soc. Rev.* **2021**, *50*, 6871–6913.
- Natraj, A.; Ji, W.; Xin, J.; Castano, I.; Burke, D. W.; Evans, A. M.; Strauss, M. J.; Ateia, M.; Hamachi, L. S.; Gianneschi, N. C.; ZA, A. L.; Sun, J.; Yusuf, K.; Dichtel, W. R. Single-Crystalline Imine-Linked Two-Dimensional Covalent Organic Frameworks Separate Benzene and Cyclohexane Efficiently. *J. Am. Chem. Soc.* **2022**, *144*, 19813–19824.



24. Wang, Z.; Zhang, S.; Chen, Y.; Zhang, Z.; Ma, S. Covalent Organic Frameworks for Separation Applications. *Chem. Soc. Rev.* **2020**, *49*, 708-735.
25. Liu, C.; Park, E.; Jin, Y.; Liu, J.; Yu, Y.; Zhang, W.; Lei, S.; Hu, W. Separation of Arylenevinylene Macrocycles with a Surface-Confining Two-Dimensional Covalent Organic Framework. *Angew. Chem. Int. Ed.* **2018**, *57*, 8984-8988.
26. Wei, P. F.; Qi, M. Z.; Wang, Z. P.; Ding, S. Y.; Yu, W.; Liu, Q.; Wang, L. K.; Wang, H. Z.; An, W. K.; Wang, W. Benzoxazole-Linked Ultrastable Covalent Organic Frameworks for Photocatalysis. *J. Am. Chem. Soc.* **2018**, *140*, 4623-4631.
27. Wang, H.; Wang, H.; Wang, Z.; Tang, L.; Zeng, G.; Xu, P.; Chen, M.; Xiong, T.; Zhou, C.; Li, X.; Huang, D.; Zhu, Y.; Wang, Z.; Tang, J. Covalent Organic Framework Photocatalysts: Structures and Applications. *Chem. Soc. Rev.* **2020**, *49*, 4135-4165.
28. Wang, G. B.; Xie, K. H.; Xu, H. P.; Wang, Y. J.; Zhao, F.; Geng, Y.; Dong, Y. B. Covalent Organic Frameworks and Their Composites as Multifunctional Photocatalysts for Efficient Visible-Light Induced Organic Transformations. *Coord. Chem. Rev.* **2022**, *472*, 214774.
29. Han, X.; Yuan, C.; Hou, B.; Liu, L.; Li, H.; Liu, Y.; Cui, Y. Chiral Covalent Organic Frameworks: Design, Synthesis and Property. *Chem. Soc. Rev.* **2020**, *49*, 6248-6272.
30. Kang, X.; Stephens, E. R.; Spector-Watts, B. M.; Li, Z.; Liu, Y.; Liu, L.; Cui, Y. Challenges and Opportunities for Chiral Covalent Organic Frameworks. *Chem. Sci.* **2022**, *13*, 9811-9832.
31. Zhang, S.; Zheng, Y.; An, H.; Aguila, B.; Yang, C. X.; Dong, Y.; Xie, W.; Cheng, P.; Zhang, Z.; Chen, Y.; Ma, S. Covalent Organic Frameworks with Chirality Enriched by Biomolecules for Efficient Chiral Separation. *Angew. Chem. Int. Ed.* **2018**, *57*, 16754-16759.
32. Qian, H. L.; Yang, C. X.; Yan, X. P., Bottom-Up Synthesis of Chiral Covalent Organic Frameworks and Their Bound Capillaries for Chiral Separation. *Nat. Commun.* **2016**, *7*, 12104.
33. Han, X.; Huang, J.; Yuan, C.; Liu, Y.; Cui, Y., Chiral 3D Covalent Organic Frameworks for High Performance Liquid Chromatographic Enantioseparation. *J. Am. Chem. Soc.* **2018**, *140*, 892-895.
34. Yan, Y. L.; Guo, D.; Wu, J. L.; Tang, X. H.; Luo, J. J.; Li, S. Q.; Fan, J.; Zheng, S. R.; Zhang, W. G.; Cai, S. L. Fabrication of Cellulose Derivative Coated Spherical Covalent Organic Frameworks as Chiral Stationary Phases for High-Performance Liquid Chromatographic Enantioseparation. *J. Chromatogr. A* **2022**, *1675*, 463155.
35. Chen, H.; Gu, Z. G.; Zhang, J. Chiral-Induced Ultrathin Covalent Organic Frameworks Nanosheets with Tunable Circularly Polarized Luminescence. *J. Am. Chem. Soc.* **2022**, *144*, 7245-7252.
36. Du, C.; Zhu, X.; Yang, C.; Liu, M. Stacked Reticular Framework Boosted Circularly Polarized Luminescence of Chiral Covalent Organic Frameworks. *Angew. Chem. Int. Ed.* **2022**, *61*, e202113979.
37. Tang, X.; Liao, X.; Cai, X.; Wu, J.; Wu, X.; Zhang, Q.; Yan, Y.; Zheng, S.; Jiang, H.; Fan, J.; Cai, S.; Zhang, W.; Liu, Y. Self-Assembly of Helical Nanofibrous Chiral Covalent Organic Frameworks. *Angew. Chem. Int. Ed.* **2023**, *62*, e202216310.
38. Gu, Q.; Zha, J.; Chen, C.; Wang, X.; Yao, W.; Liu, J.; Kang, F.; Yang, J.; Li, Y.; Lei, D.; Tang, Z.; H. Y.; Tan, C.; Zhang, Q. Constructing Chiral Covalent-Organic Frameworks for Circularly Polarized Light Detection. *Adv. Mater.* **2023**, 2306414.
39. Yue, J. Y.; Song, L. P.; Shi, Y. H.; Zhang, L.; Pan, Z. X.; Yang, P.; Ma, Y.; Tang, B. Chiral Ionic Covalent Organic Framework as an Enantioselective Fluorescent Sensor for Phenylalaninol Determination. *Anal. Chem.* **2023**, *95*, 11078-11084.
40. Wu, X.; Han, X.; Xu, Q.; Liu, Y.; Yuan, C.; Yang, S.; Liu, Y.; Jiang, J.; Cui, Y. Chiral BINOL-Based Covalent Organic Frameworks for Enantioselective Sensing. *J. Am. Chem. Soc.* **2019**, *141*, 7081-7089.
41. Qin, S.; You, X.; Guo, X.; Chu, H.; Dong, Q.; Cui, H.; Jin, F.; Gao, L. A Chiral Fluorescent COF Prepared by Post-Synthesis Modification for Optosensing of Imazamox Enantiomers. *Spectrochim. Acta A Mol. Biomol. Spectrosc.* **2023**, *291*, 122370.
42. Zheng, Z.; Yuan, C.; Sun, M.; Dong, J.; Liu, Y.; Cui, Y. Construction of Monophosphine-Metal Complexes in Privileged Diphosphine-Based Covalent Organic Frameworks for Catalytic Asymmetric Hydrogenation. *J. Am. Chem. Soc.* **2023**, *145*, 6100-6111.
43. Zhang, J.; Han, X.; Wu, X.; Liu, Y.; Cui, Y. Multivariate Chiral Covalent Organic Frameworks with Controlled Crystallinity and Stability for Asymmetric Catalysis. *J. Am. Chem. Soc.* **2017**, *139*, 8277-8285.
44. Xu, H. S.; Ding, S. Y.; An, W. K.; Wu, H.; Wang, W. Constructing Crystalline Covalent Organic Frameworks from Chiral Building Blocks. *J. Am. Chem. Soc.* **2016**, *138*, 11489-11492.
45. Kan, X.; Wang, J. C.; Chen, Z.; Du, J. Q.; Kan, J. L.; Li, W. Y.; Dong, Y. B. Synthesis of Metal-Free Chiral Covalent Organic Framework for Visible-Light-Mediated Enantioselective Photooxidation in Water. *J. Am. Chem. Soc.* **2022**, *144*, 6681-6686.
46. Chen, M.; Zhang, J.; Liu, C.; Li, H.; Yang, H.; Feng, Y.; Zhang, B. Construction of Pyridine-Based Chiral Ionic Covalent Organic Frameworks as a Heterogeneous Catalyst for Promoting Asymmetric Henry Reactions. *Org. Lett.* **2021**, *23*, 1748-1752.
47. Xu, H.; Gao, J.; Jiang, D. Stable, Crystalline, Porous, Covalent Organic Frameworks as a Platform for Chiral Organocatalysts. *Nat. Chem.* **2015**, *7*, 905-912.
48. Das, G.; Benyettou, F.; Sharma, S. K.; Sharama, S. K.; Prakasam, T.; Gandara, F.; de la Pen-O'Shea, V. A.; Saleh, N.; Pasricha, R.; Jagannathan, R.; Olson, M. A.; Trabolsi, A. Covalent Organic Nanosheets for Bioimaging. *Chem. Sci.* **2018**, *9*, 8382-8387.
49. Krishnaraj, C.; Kaczmarek, A. M.; Jena, H. S.; Leus, K.; Chaoui, N.; Schmidt, J.; Van Deun, R.; Van Der Voort, P. Triggering White-Light Emission in a 2D Imine Covalent Organic Framework Through Lanthanide Augmentation. *ACS Appl. Mater. Interfaces* **2019**, *11*, 27343-27352.
50. Das, G.; Prakasam, T.; Alkhatib, N.; AbdulHalim, R. G.; Chandra, F.; Sharma, S. K.; Garai, B.; Varghese, S.; Addicoat, M. A.; Ravaux, F.; Pasricha, R.; Jagannathan, R.; Saleh, N.; Kirmizialtin, S.; Olson, M. A.; Trabolsi, A. Light-Driven Self-Assembly of Spiropyran-Functionalized Covalent Organic Framework. *Nat. Commun.* **2023**, *14*, 3765.
51. Li, Z.; Li, H.; Guan, X.; Tang, J.; Yusran, Y.; Li, Z.; Xue, M.; Fang, Q.; Yan, Y.; Valtchey, V.; Qiu, S. Three-Dimensional Ionic Covalent Organic Frameworks for Rapid, Reversible, and Selective Ion Exchange. *J. Am. Chem. Soc.* **2017**, *139*, 17771-17774.
52. Sakthivel, K.; Notz, W.; Bui, T.; Barbas, C. F. Amino Acid Catalyzed Direct Asymmetric Aldol Reactions: A Bioorganic Approach to Catalytic Asymmetric Carbon-Carbon Bond-Forming Reactions. *J. Am. Chem. Soc.* **2001**, *123*, 5260-5267.
53. List, B.; Lerner, R. A.; Barbas, C. F. Proline-Catalyzed Direct Asymmetric Aldol Reactions. *J. Am. Chem. Soc.* **2000**, *122*, 2395-2396.
54. Zhang, Y.; Guo, J.; Zhang, J.; Qiu, X.; Zhang, X.; Han, J.; Zhang, B.; Long, C.; Shi, Y.; Yang, Z.; Zhao, W.; Tang, Z. Metal-Organic Frameworks Enable Regio- and Stereo-Selective Functionalization of Aldehydes and Ketones. *Chem.* **2022**, *8*, 1688-1704.
55. Nguyen, K. D.; Ehrling, S.; Senkovska, I.; Bon, V.; Kaskel, S. New 1D Chiral Zr-MOFs Based on in Situ Imine Linker Formation as Catalysts for Asymmetric C-C Coupling Reactions. *J. Catal.* **2020**, *386*, 106-116.

56. Feng, X.; Jena, H. S.; Leus, K.; Wang, G.; Ouwehand, J.; Van Der Voort, P. L-Proline Modulated Zirconium Metal Organic Frameworks: Simple Chiral Catalysts for the Aldol Addition Reaction. *J. Catal.* **2018**, *365*, 36-42.
57. Kutzscher, C.; Nickerl, G.; Senkowska, I.; Bon, V.; Kaskel, S. Proline Functionalized UiO-67 and UiO-68 Type Metal-Organic Frameworks Showing Reversed Diastereoselectivity in Aldol Addition Reactions. *Chem. Mater.* **2016**, *28*, 2573-2580.
58. Liu, Y.; Xi, X.; Ye, C.; Gong, T.; Yang, Z.; Cui, Y. Chiral Metal-Organic Frameworks Bearing Free Carboxylic Acids for Organocatalyst Encapsulation. *Angew. Chem. Int. Ed.* **2014**, *53*, 13821-13825.
59. Dang, D.; Wu, P.; He, C.; Xie, Z.; Duan, C. Homochiral Metal-Organic Frameworks for Heterogeneous Asymmetric Catalysis. *J. Am. Chem. Soc.* **2010**, *132*, 14321-14323.
60. Banerjee, M.; Das, S.; Yoon, M.; Choi, H. J.; Hyun, M. H.; Park, S. M.; Seo, G.; Kim, K. Postsynthetic Modification Switches an Achiral Framework to Catalytically Active Homochiral Metal-Organic Porous Materials. *J. Am. Chem. Soc.* **2009**, *131*, 7524-7525.

## Table of Contents

